Journal of Materials Chemistry C

PAPER

View Article Online
View Journal | View Issue

Cite this: J. Mater. Chem. C, 2018, 6, 7361

Pure red upconversion luminescence and optical thermometry of Er^{3+} doped sensitizer-rich $SrYbInO_4$ phosphors

Ningzi Zhang,[a] Maxim S. Molokeev,[bcd] Quanlin Liu[a] and Zhiguo Xia*[a]

Received 26th May 2018,
Accepted 18th June 2018

DOI: 10.1039/c8tc02565g

rsc.li/materials-c

Er^{3+} doped sensitizer-rich $SrYbInO_4$ upconversion phosphors with an orthorhombic structure (*Pnma*) were synthesized by using a high temperature solid state reaction and their phase structure, site occupation and microstructure have been analyzed. Interestingly, upon the excitation from 980 nm pulsed laser diodes, the $SrYbInO_4$:Er^{3+} phosphor emitted a nearly pure red emission on account of the $^4F_{9/2} \rightarrow {}^4I_{15/2}$ transition of Er^{3+}. Additionally, based on the pump power dependence of the upconversion intensity and the schematic diagram of the energy levels, the upconversion mechanism in this system was verified in a two-photon process. The temperature-dependent behaviors of the as-synthesized sample demonstrated the potential for applications in optical thermometry.

Introduction

Lanthanide ion doped upconversion phosphors have attracted much attention owing to their unique photophysical characteristics, making them feasible for a large number of applications in solid state lasers, solar cell conversion, sensor techniques, bioimaging, colour display, drug delivery, *etc.*[1–12] Rare earth ions with f–f transitions, especially Er^{3+} ions, are frequently employed by upconversion luminescent materials as activators due to their abundant electronic states and ladder-like energy levels.[13] Yb^{3+} ions typically act as sensitizers in the upconversion process by virtue of a large absorption cross-section in the near infrared region, for example, Yb^{3+} ions perform the energy transfer with Er^{3+} ions to achieve the enhancement of upconversion luminescence intensity upon 980 nm excitation.[14,15] It is well known that a suitable host for upconversion phosphors should have a low phonon energy. Amongst these, MIn_2O_4 (M = Ca, Sr) has previously been proved to be a good oxide host with great chemical stability and low phonon energy.[13,16] $SrIn_2O_4$ has an orthorhombic structure of the $CaFe_2O_4$ type with the *Pnam* space group, and $CaIn_2O_4$ has the same structure, but with a different space group, $Pca2_1$ or *Pbcm*. Accordingly, rare earth ion doped $CaIn_2O_4$ or $SrIn_2O_4$ upconversion phosphors have been extensively reported in recent years. However, in 2017, Ayaka Fujimoto *et al.* reported $SrYbInO_4$ as the first example of a pure oxide-ion conductor with a $CaFe_2O_4$-type structure.[17] In this investigation, we report a kind of special sensitizer-rich (Yb^{3+}) new material, $SrYbInO_4$:Er^{3+} upconversion phosphors, with pure far red emission at around 670 nm, which is also different from that of the Er^{3+} doped $SrIn_2O_4$ phosphors.[16] Besides, the good performance of temperature sensing behavior makes this novel phosphor a candidate in optical thermometry.

As is well known, temperature is an important parameter in a majority of fields, such as scientific research, industrial manufacture and fire protection.[14] It is noteworthy that compared with traditional temperature sensors, optical thermometry provides a noncontact thermal measurement technology, which can detect the temperature at a distance from the material. In particular, optical temperature sensing is extremely suitable for temperature detection in some harsh environments, such as coal mines, electrical power stations, building fires and so on.[15] Hence, exploring a suitable upconversion luminescent material is highly desired for optical temperature sensors. To the best of our knowledge, pure red emission *via* the upconversion process makes a material a suitable candidate for *in vivo* imaging.[18] Based on the Yb^{3+}/Er^{3+} system, it is noted that the intensity of the red emission centred at 670 nm greatly depends on the upconversion host materials.[19] Fluorides with low phonon energies are typical upconversion host materials and have achieved enhanced red emission upon 980 nm excitation, for example, β-$NaYF_4$,[19] KSc_2F_7,[20] $NaYbF_4$,[21] $Ca_{0.65}La_{0.35}F_{2.35}$ and so on.[22] Some oxides represented by Y_2O_3 could also produce intense red emission though upconversion. Additionally, Wu *et al.* reported $Ba_5Gd_8Zn_4O_{21}$ and $Ba_3Y_4O_9$ with strong red emission.[19,23]

[a] The Beijing Municipal Key Laboratory of New Energy Materials and Technologies, School of Materials Sciences and Engineering, University of Science and Technology Beijing, Beijing 100083, China. E-mail: xiazg@ustb.edu.cn; Fax: +86-10-82377955; Tel: +86-10-82377955
[b] Laboratory of Crystal Physics, Kirensky Institute of Physics, Federal Research Center KSC SB RAS, Krasnoyarsk 660036, Russia
[c] Siberian Federal University, Krasnoyarsk, 660041, Russia
[d] Department of Physics, Far Eastern State Transport University, Khabarovsk, 680021, Russia

According to the literature,[21,24,25] the boost in red emission yield is generally attributed to the collaborative effect of high sensitizer concentration and cross relaxation between activators. Additionally, the scatted light, absorbance, and autofluorescence of biological tissues could be minimized in the optical window, for which the range is the near infrared region (700–1100 nm) and the red region (600–700 nm). Hence, an upconversion material, where the excitation and emission wavelengths are both included in the optical window, is also necessary for *in vivo* imaging and non-contact thermal measurement.

Thus, the special sensitizer-rich $SrYbInO_4$:Er^{3+} upconversion phosphors have been investigated in this paper, and the pure red emission *via* the upconversion process, as well as their temperature sensor applications, has been demonstrated.

Experimental section

Chemicals

$SrCO_3$ (99%, A.R.), Yb_2O_3 (99.9%), In_2O_3 (99.9%) and Er_2O_3 (99.99%) were commercially purchased from Aladdin. All the chemicals were used as received without any further purification.

Synthesis

A series of Er^{3+} ion doped $SrYbInO_4$ phosphors was synthesized *via* a high temperature solid reaction. $SrCO_3$, Yb_2O_3, In_2O_3 and Er_2O_3 were used as raw materials. The required cation sources as the starting materials were weighed and mixed in the given stoichiometric proportion. Subsequently, all the mixed starting materials were ground together with a small amount of alcohol for about half an hour using an agate mortar and pestle until the mixtures were almost dry. Then, the mixtures were placed in alumina crucibles. The powder mixtures were first sintered in air at 1000 °C for 5 h and cooled to room temperature. After a second homogenization in the mortar, the samples were calcined again at 1400 °C for 5 h in the furnace. The obtained samples were ground into powders for the following measurements.

Characterization

The powder X-ray diffraction (XRD) patterns of the samples were measured using a D8 Advance diffractometer (Bruker Corporation, Germany) operating at 40 kV and 40 mA with monochromatized Cu Kα radiation (λ = 1.5406 Å). A continuous-scanning mode with a scanning rate of 8° min^{-1} for phase identification was adopted with a 2θ range from 10° to 70°. The powder diffraction patterns of $SrYbInO_4$ for Rietveld analysis were collected with the same powder diffractometer. The step size of 2θ was 0.013°, and the counting time was 2 s per step. The test range of 2θ was from 5° to 120°. Rietveld refinements were performed by using TOPAS 4.2 software.[26] The morphology, the crystalline size and elemental mapping of the as-prepared phosphors were characterized at room temperature using scanning electron microscopy (SEM, JEOL JSM-6510). The room-temperature upconversion photoluminescence spectra were recorded by using a fluorescence spectrophotometer (F-4600, HITACHI, Japan) equipped with an external 980 nm semiconductor laser with controlled power as the excitation source, which is connected with an optic fiber accessory. The temperature-dependent spectra were measured on the same device, which was coupled with a heating attachment and an electric furnace controlled by a computer.

Results and discussion

Structural characterization of $SrYbInO_4$:Er^{3+} samples

The XRD patterns of the Er^{3+} doped $SrYbInO_4$ samples with different concentrations of Er^{3+} are shown in Fig. 1. It was found that the XRD patterns of the as-prepared samples agree well with the simulated pattern using the crystallographic data of $SrYbInO_4$, and the doping of Er^{3+} does not change the phase structures. Compared with the standard pattern of $SrIn_2O_4$, all diffraction peaks move to smaller angles. Moreover, Fig. 2a illustrates the difference Rietveld refinement plot of the selected $SrYbInO_4$:0.05Er^{3+}. All peaks besides the small impurity peaks of Yb_2O_3 (~2 wt%) were indexed by the orthorhombic cell (*Pnma*) with parameters close to $SrYbInO_4$ on account of the Rietveld refinement results.[17] Therefore, this crystal structure was taken as the starting model for Rietveld refinement. According to the literature,[27,28] the structural features of MIn_2O_4 (M = Ca, Sr) include an eight-coordinated Ca or Sr ion and two different types of InO_6 double octahedra to form a pentagonal prism-like tunnel network structure. Compared with the structure of MIn_2O_4, two Yb/In sites with partial occupational disorder take the place of In ions of MIn_2O_4 in the structure of $SrYbInO_4$, as shown in Fig. 2b.[17] We also refined their occupancies with the suggestion occ(Yb) + occ(In) = 1 in each site. Additionally, the ratio of all Yb ions to all In ions was restrained to Yb/In = 1 : 1. The refinement was stable and gave low *R*-factors, as seen in Table 1 and Fig. 2a. The coordinates of atoms and the main bond lengths are shown in Tables 2 and 3, respectively. The cell volume of the doped compound $SrYbInO_4$:0.05Er^{3+}, V = 382.516(4) $Å^3$, is bigger than the cell volume of the host, V = 382.03 $Å^3$, which is in good agreement with the fact that the Er ion radius, IR (Er^{3+}, CN = 6) = 0.89 Å, is bigger than the ion radius of the Yb ion, IR (Yb^{3+}, CN = 6) = 0.868 Å.

The morphology and the particle size act as two significant factors for the optimization of the luminescence properties of

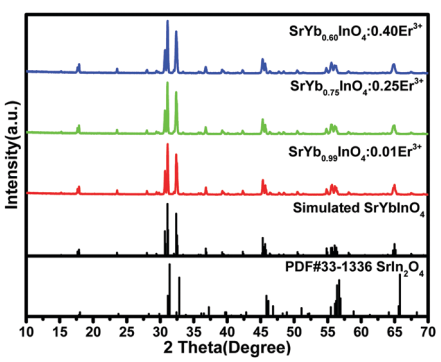

Fig. 1 Powder XRD patterns of $SrYb_{1-x}InO_4$:xEr^{3+} with different concentrations of Er^{3+}, and the simulated patterns of $SrYbInO_4$ and PDF #33-1336 are also given as a comparison.

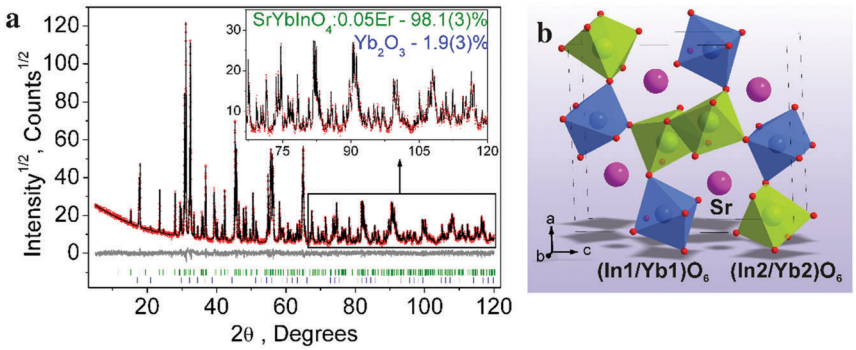

Fig. 2 (a) Rietveld refinement XRD pattern of $SrYbInO_4$:0.05Er^{3+} showing the pure phase of $SrYbInO_4$ and a small amount of impurity of Yb_2O_3. (b) Typical crystal structure of $SrYbInO_4$ highlighting the two polyhedra, $(Yb1/In1)O_6$ and $(Yb2/In2)O_6$.

Table 1 Main parameters of the processing and refinement of the $SrYbInO_4$:0.05Er sample

Phase	Weight (%)	Space group	Cell parameters (°, Å), Cell volume (Å^3)	R_{wp}, R_p (%), χ^2	R_B (%)
$SrYbInO_4$:0.05Er	98.1(3)	*Pnma*	a = 9.91968(6), b = 3.31135(2), c = 11.64519(7), V = 382.516(4)	8.52, 5.97, 1.27	1.91
Yb_2O_3	1.9(3)	$Ia\bar{3}$	a = 10.3839(3), V = 1119.7(1)		2.12

Table 2 Fractional atomic coordinates and isotropic displacement parameters (Å^2) of $SrYbInO_4$:0.05Er

	x	y	Z	B_{iso}	Occ.
Sr	0.75345(14)	1/4	0.34850(11)	0.68(5)	1
In1	0.4210(1)	1/4	0.89188(7)	0.48(5)	0.574(8)
Yb1	0.4210(1)	1/4	0.89188(7)	0.48(5)	0.426(8)
In2	0.42647(9)	1/4	0.38837(7)	0.63(5)	0.426(8)
Yb2	0.42647(9)	1/4	0.38837(7)	0.63(5)	0.574(8)
O1	0.2129(9)	1/4	0.8315(7)	0.7(1)	1
O2	0.1192(8)	1/4	0.5211(7)	0.7(1)	1
O3	0.5195(9)	1/4	0.2198(7)	0.7(1)	1
O4	0.425(1)	1/4	0.5764(6)	0.7(1)	1

Table 3 Main bond lengths (Å) of $SrYbInO_4$:0.05Er

Sr–O1^{i}	2.692(7)	(In1/Yb1)–O1	2.181(9)
Sr–O2^{i}	2.578(6)	(In1/Yb1)–O2^{iii}	2.272(6)
Sr–O3	2.763(9)	(In1/Yb1)–O2^{iv}	2.212(8)
Sr–O3^{ii}	2.756(9)	(In1/Yb1)–O3^{i}	2.186(5)
Sr–O4^{i}	2.577(7)	(In2/Yb2)–O1^{v}	2.256(6)
		(In2/Yb2)–O3	2.170(8)
		(In2/Yb2)–O4	2.189(7)
		(In2/Yb2)–O4^{i}	2.254(7)

Symmetry codes: (i) $-x+1, -y, -z+1$; (ii) $x+1/2, -y+1/2, -z+1/2$; (iii) $-x+1/2, -y, z+1/2$; (iv) $x+1/2, -y+1/2, -z+3/2$; (v) $-x+1/2, -y, z-1/2$.

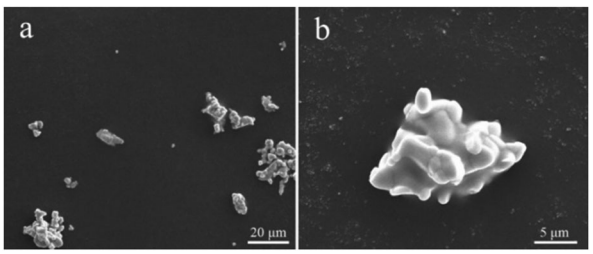

Fig. 3 SEM images of Er^{3+} doped $SrYbInO_4$ phosphor with different magnifications.

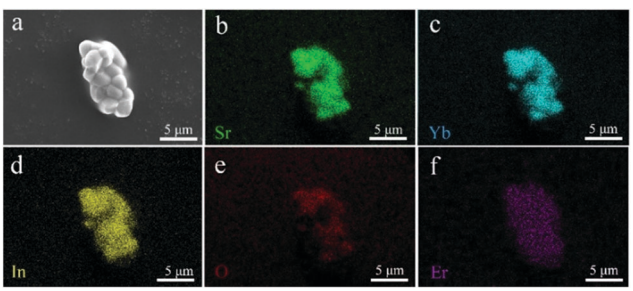

Fig. 4 SEM image (a) of $SrYbInO_4$:Er^{3+} along with elemental mapping for different elements: Sr (b), Yb (c), In (d), O (e), and Er (f).

phosphor materials. Therefore, the scanning electron microscopy (SEM) measurement was characterized and Fig. 3 demonstrates the representative SEM images of the as-synthesized $SrYbInO_4$:Er^{3+} phosphors under different magnifications. In Fig. 3, it is clear that the $SrYbInO_4$:Er^{3+} samples have irregular shapes with an average particle size of ~3 μm. As further exhibited in Fig. 4, the elemental mapping of Sr, Yb, In, O and Er on the $SrYbInO_4$:Er^{3+} up-conversion phosphor confirms that all the elements are uniformly distributed and the doped Er^{3+} ion has successfully entered the crystal lattice of $SrYbInO_4$ uniformly, as also confirmed by the Rietveld refinement results.

Upconversion luminescence properties of $SrYbInO_4$:Er^{3+} samples

To investigate the upconversion luminescence properties and the influence of Er^{3+} ion concentration on the emission behaviors of the as-synthesized samples under 980 nm excitation, the upconversion emission spectra of $SrYbInO_4$:Er^{3+} powder with different concentrations of Er^{3+} ions are given in Fig. 5. As shown in Fig. 5a, it is evident that the $SrYbInO_4$:Er^{3+} phosphor mainly emitted red emission with an intensity peak at around 670 nm, which originated from the $^4F_{9/2} \rightarrow {}^4I_{15/2}$ transitions of Er^{3+}. It is

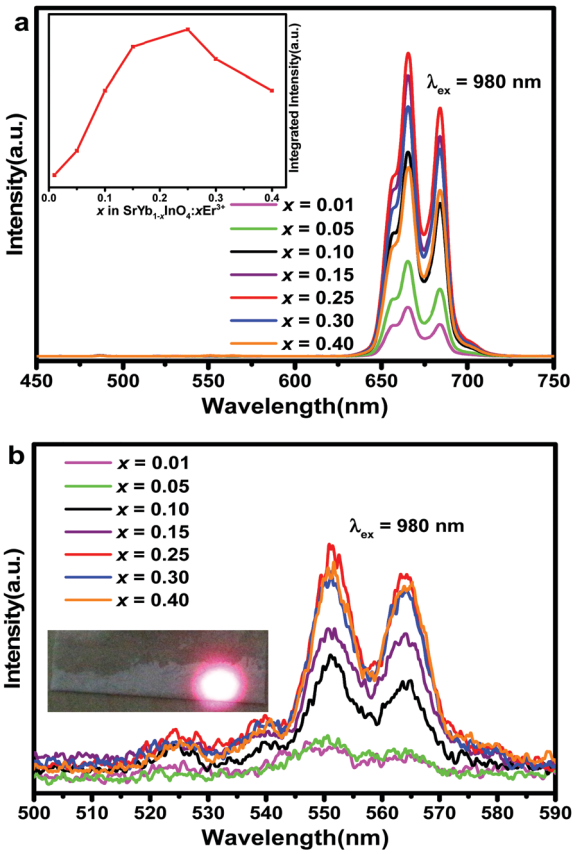

Fig. 5 (a) The up-conversion spectra of $SrYb_{1-x}InO_4$: xEr^{3+} with different concentrations of Er^{3+} ion. The inset presents the variations of the red up-conversion emission intensities *versus* Er^{3+} concentration. (b) The up-conversion spectra of $SrYb_{1-x}InO_4$:xEr^{3+} ranging from 500 nm to 590 nm at ×250 magnification. The inset presents the photograph of the sample excited by using a 980 nm laser diode.

interesting to find that green emissions with peaks at about 525 nm and 550 nm were extremely weak, even negligible, and a nearly pure red emission can be found from the spectrum. The inset of Fig. 5a illustrates the integrated intensity of the red emission as a function of the activator Er^{3+} doping concentration. It was observed that the red emission intensity increased gradually with the increase of Er^{3+} content and reached a maximum when the concentration of Er^{3+} was 0.25. Subsequently, there appeared a decrease in the luminescence intensity as the Er^{3+} content continued to increase beyond 0.25 due to the concentration quenching effect.[29] This effect should be ascribed to the energy transfer between the adjacent Er^{3+} and Yb^{3+} ions or Er^{3+} and Er^{3+} ions.[13] In principle, the energy transfer from the host to the Er^{3+} ion, which was induced by a lower Er^{3+} content, could facilitate the radiative transition and further result in the elevation of photoluminescence. Nevertheless, most interactions between rare earth ions are proportional to r^{-6}, where r is the distance (r) between the ions. The reduction of the distance facilitates the energy transfer.[27] Obviously, along with the elevation of Er^{3+} concentration, the decrease of the distance between the nearest Er^{3+} and Yb^{3+} or Er^{3+} ions will facilitate non-radiative energy transfer, which could result in the eventual reduction of the upconversion luminescence intensity. Fig. 5b displays the upconversion luminescence spectra ranging from 500 nm to 590 nm at ×250 magnification. It can be observed that the green emission bands centered at around 525 nm and 550 nm are too weak to be visible to the naked eye. The digital photograph of the sample excited by a 980 nm IR laser diode also demonstrates a strong red emission due to the negligible green emission, as also confirmed by the emission spectra in Fig. 5a.

Upconversion luminescence mechanism analysis

The dependence of upconversion luminescence intensity on pump power was investigated in order to understand the up-conversion luminescence mechanisms, as depicted in Fig. 6a. It is obvious that along with the enhancement of pump power, the red emission intensity increases. As is well known, for the unsaturated upconversion luminescence process, the upconversion intensity I is related to the pumping laser power P as follows:[30]

$$I \propto P^n$$

where n is the number of pumping photons absorbed by rare earth ions at the ground state that subsequently transit to the upper excited state. The inset of Fig. 6a shows the Ln–Ln plot of the integrated red emission intensity as a function of the excitation power for the as-studied $SrYbInO_4$:Er^{3+} sample. The amount of photons n is found to be around 1.615, which is calculated from the slope of this fitted straight line. Consequently, the upconversion red

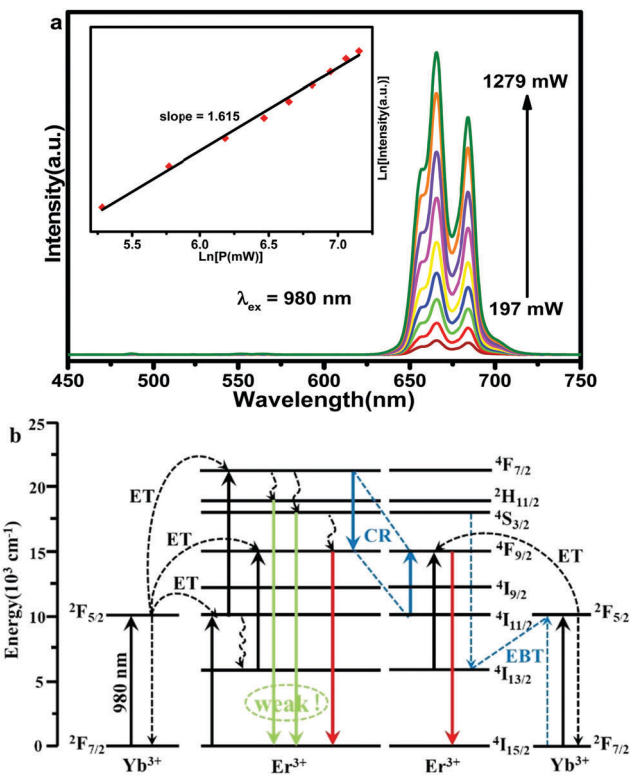

Fig. 6 (a) Visible UC emission spectra of $SrYb_{0.75}InO_4$:$0.25Er^{3+}$. The inset presents the pump power dependence of the UC emission intensities in the Er^{3+} doped $SrYbInO_4$ phosphor. (b) Schematic energy level diagram of Er^{3+} in the $SrYbInO_4$ system.

emission in Er^{3+} doped $SrYbInO_4$ samples is determined to be involved in a two-photon process.

In the sensitizer-rich $SrYbInO_4$ host, Yb^{3+} ions not only help to form the crystal structure, but also act as the sensitizer of the upconversion process. To further illustrate the upconversion mechanism, the schematic diagram of the energy levels of Yb^{3+} and Er^{3+} ions and possible transitions of the Er^{3+} doped $SrYbInO_4$ samples upon 980 nm excitation are proposed as shown in Fig. 6b. First of all, the Yb^{3+} ion is elevated from the ground state $^2F_{7/2}$ to $^2F_{5/2}$ energy level by absorbing one infrared photon with 980 nm wavelength. Then, the energy transfer (ET) between the sensitizer Yb^{3+} ion and the activator Er^{3+} ion occurs because $^2F_{5/2}$ of the Yb^{3+} ion and $^4I_{11/2}$ of the Er^{3+} ion are syntonic, which induces an electron transition from $^4I_{15/2}$ to $^4I_{11/2}$ of Er^{3+}.[31] Subsequently, electrons at the $^4I_{11/2}$ level could partly relax to the $^4I_{13/2}$ level by a non-radiative relaxation process. The reason for the nearly pure red emission can be explained as follows: the populations of the $^4I_{13/2}$ and $^4I_{11/2}$ levels are excited to the $^4F_{9/2}$ and $^4F_{7/2}$ levels by the subsequent ET process. The transitions from the $^4F_{9/2}$ to $^4I_{15/2}$ level occur with the red emission. Also, the population of $^2H_{11/2}$ and $^3S_{3/2}$ levels would be populated by non-radiative relaxation at the $^4F_{7/2}$ level. Part of the population of the $^3S_{3/2}$ level is relaxed to the $^4F_{9/2}$ state, which also generates the transition from the $^4F_{9/2}$ to $^4I_{15/2}$ level with the red emission. In general, it produces the transitions from $^2H_{11/2}$ and $^3S_{3/2}$ to the $^4I_{15/2}$ level along with the weak green emissions.[19] Yet, in this upconversion system, the cross relaxation (CR) process ($^4F_{7/2} + {}^4I_{11/2} \rightarrow 2{}^4F_{9/2}$) plays a dominant role instead of non-radiative relaxation.[21,22] Further, there exists the energy back transfer (EBT) process from Er^{3+} to Yb^{3+} ($^4S_{3/2} + {}^2F_{7/2} \rightarrow {}^4I_{13/2} + {}^2F_{5/2}$) with a high concentration of Yb^{3+} ions.[32,33] What is discussed above could cause a reduction of the population at the $^4S_{3/2}$ and $^4F_{7/2}$ levels and an increase at the $^4I_{13/2}$ and $^4F_{9/2}$ levels. As a result, the red emission intensity is enhanced. Conversely, the green emissions are extremely weak.

Optical thermometry application

We know that the fluorescence intensity ratio (FIR) technique from two different emission centres has become a hot issue, and it relates to a high relative sensitivity. However, autofluorescence of biological tissues could be minimized in the optical window, for which the range is the near infrared region (700–1100 nm) and the red region (600–700 nm), and it will be efficient if the pure red emission is investigated as an optical thermometry application. Herein, in order to investigate the temperature sensing behaviour of the as-synthesized materials, the temperature-dependent upconversion spectra were obtained in the temperature range between 40 °C and 240 °C, as shown in Fig. 7. It is apparent that the peak position of the red emission band does not shift and the intensity of the red emission decreases obviously with increasing temperature. The inset of Fig. 7 illustrates the plot of the integrated intensity from the red emission as a function of absolute temperature. As can be seen from the line fit, the slope of the near-linear curve is equal to −117.92. Moreover, the sensitivity is related to the ratio between the slope and the integrated intensity, and the variation of sensitivity with

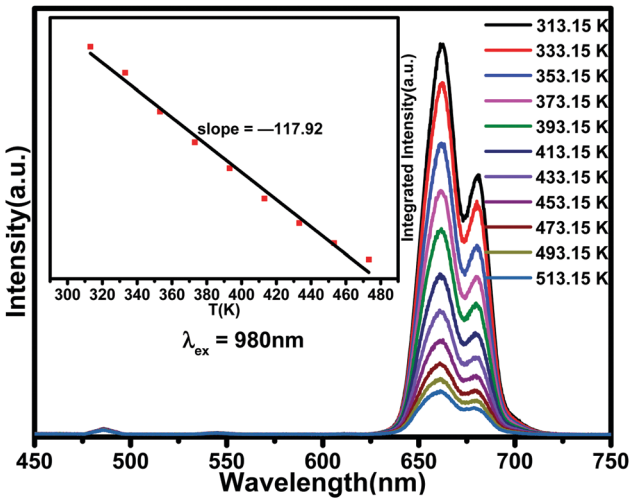

Fig. 7 Temperature-dependence spectra of $SrYb_{0.75}InO_4$:0.25Er^{3+} samples. The inset presents the plot of the intensity of I_{670} as a function of the temperature.

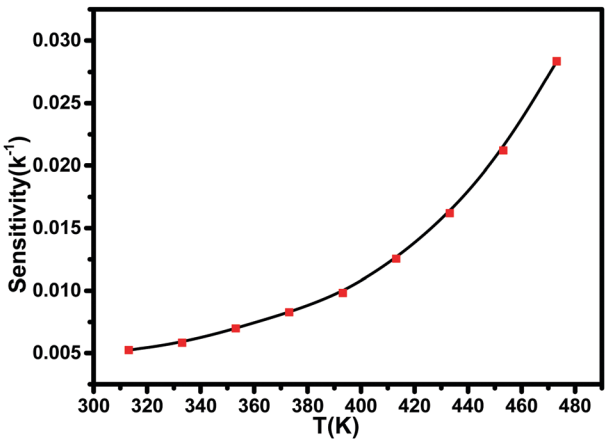

Fig. 8 The variation of sensitivity with temperature of $SrYb_{0.75}InO_4$:0.25Er^{3+} samples.

temperature is shown in Fig. 8. It is found that the sensitivity parameter increases with temperature from 0.005 K^{-1} at 313.15 K to 0.028 K^{-1} at 513.15 K, due to the influence of the integrated intensity. Therefore, it is possible for Er^{3+} doped $SrYbInO_4$ phosphors to be applied in the temperature sensing field. Also, this material has potential applications in non-contact thermal measurement, which is necessary in some harsh environments.[34]

Conclusions

In summary, Er^{3+} doped sensitizer-rich $SrYbInO_4$ phosphors were successfully synthesized by a conventional solid state reaction. The powder XRD pattern from Rietveld refinement revealed that the final sample was the Sr(Yb,Er)InO_4 phase with an orthorhombic $CaFe_2O_4$-type structure (*Pnma*). As for the luminescence properties, the optimum doping concentration of the Er^{3+} ion was studied, which is equal to 0.25. Also, there

exists a pure red emission corresponding to the transition from the $^4F_{9/2}$ to $^4I_{15/2}$ level of Er^{3+} in the sample, and the upconversion luminescence mechanism was investigated in detail, in which the cross relaxation process was dominant. Eventually, the temperature-dependent properties of the samples gave evidence for the potential application in optical thermometry as pure red emission.

Conflicts of interest

There are no conflicts to declare.

Acknowledgements

The present work was supported by the National Natural Science Foundation of China (Grant 91622125, 51722202 and 51572023) and the Natural Science Foundations of Beijing (2172036), and M. Molokeev acknowledges support of the Russian Foundation for Basic Research (17-52-53031).

Notes and references

1 D. Chen and P. Huang, *Dalton Trans.*, 2014, **43**, 11299–11304.
2 M. Ding, D. Chen, T. Chen, C. Lu, Y. Ni and Z. Xu, *Mater. Lett.*, 2014, **128**, 101–104.
3 X. Huang, S. Han, W. Huang and X. Liu, *Chem. Soc. Rev.*, 2013, **42**, 173–201.
4 W. Luo, Y. Liu and X. Chen, *Sci. China Mater.*, 2015, **58**, 819–850.
5 B. M. van der Ende, L. Aarts and A. Meijerink, *Phys. Chem. Chem. Phys.*, 2009, **11**, 11081–11095.
6 F. Wang and X. Liu, *Chem. Soc. Rev.*, 2009, **38**, 976–989.
7 W. Yu, W. Xu, H. Song and S. Zhang, *Dalton Trans.*, 2014, **43**, 6139–6147.
8 Q. Ju, D. Tu, Y. Liu, R. Li, H. Zhu, J. Chen, Z. Chen, M. Huang and X. Chen, *J. Am. Chem. Soc.*, 2012, **134**, 1323–1330.
9 J. Zhou, Q. Liu, W. Feng, Y. Sun and F. Li, *Chem. Rev.*, 2015, **115**, 395–465.
10 F. Wang, D. Banerjee, Y. Liu, X. Chen and X. Liu, *Analyst*, 2010, **135**, 1839–1854.
11 G. Tian, W. Ren, L. Yan, S. Jian, Z. Gu, L. Zhou, S. Jin, W. Yin, S. Li and Y. Zhao, *Small*, 2013, **9**, 1929–1938.
12 G. Yi, Y. Peng and Z. Gao, *Chem. Mater.*, 2011, **23**, 2729–2734.
13 T. Li, C. Guo and L. Li, *Opt. Express*, 2013, **21**, 18281–18289.
14 Y. Zhang, X. Chai, J. Li, X. Wang, Y. Li and X. Yao, *J. Alloys Compd.*, 2018, **735**, 473–479.
15 Y. Tian, B. Tian, C. Cui, P. Huang, L. Wang and B. Chen, *RSC Adv.*, 2015, **5**, 14123–14128.
16 M. Guan, H. Zheng, L. Mei, M. S. Molokeev, J. Xie, T. Yang, X. Wu, S. Huang, Z. Huang and A. Setlur, *J. Am. Ceram. Soc.*, 2015, **98**, 1182–1187.
17 A. Fujimoto, M. Yashima, K. Fujii and J. R. Hester, *J. Phys. Chem. C*, 2017, **121**, 21272–21280.
18 G. Tian, Z. Gu, L. Zhou, W. Yin, X. Liu, L. Yan, S. Jin, W. Ren, G. Xing, S. Li and Y. Zhao, *Adv. Mater.*, 2012, **24**, 1226–1231.
19 H. Wu, Z. Hao, L. Zhang, X. Zhang, Y. Xiao, G.-H. Pan, H. Wu, Y. Luo, H. Zhao and J. Zhang, *J. Phys. Chem. C*, 2018, **122**, 9611–9618.
20 Y. Ding, X. Teng, H. Zhu, L. Wang, W. Pei, J. J. Zhu, L. Huang and W. Huang, *Nanoscale*, 2013, **5**, 11928–11932.
21 W. Wei, Y. Zhang, R. Chen, J. Goggi, N. Ren, L. Huang, K. K. Bhakoo, H. Sun and T. T. Y. Tan, *Chem. Mater.*, 2014, **26**, 5183–5186.
22 P. Du, Z. Xia and L. Liao, *Mater. Res. Bull.*, 2011, **46**, 543–546.
23 H. Wu, Z. Hao, L. Zhang, X. Zhang, Y. Xiao, G.-H. Pan, H. Wu, Y. Luo, L. Zhang and J. Zhang, *J. Phys. Chem. C*, 2018, **6**, 3459–3467.
24 M. Pollnau, D. R. Gamelin, S. R. Luthi, H. U. Gudel and M. P. Hehlen, *Phys. Rev. B: Condens. Matter Mater. Phys.*, 2000, **61**, 3337–3346.
25 P. S. Golding, S. D. Jackson, T. A. King and M. Pollnau, *Phys. Rev. B: Condens. Matter Mater. Phys.*, 2000, **62**, 856–864.
26 *Bruker AXS TOPAS V4: General profile and structure analysis software for powder diffraction data-User's Manual*, Bruker AXS, Karlsruhe, Germany, 2008.
27 T. Li, C.-F. Guo, Y.-M. Yang, L. Li and N. Zhang, *Acta Mater.*, 2013, **61**, 7481–7487.
28 X. M. Liu, C. X. Li, Z. W. Quan, Z. Y. Cheng and J. Lin, *J. Phys. Chem. C*, 2007, **111**, 16601–16607.
29 B. P. Singh, A. K. Parchur, R. S. Ningthoujam, P. V. Ramakrishna, S. Singh, P. Singh, S. B. Rai and R. Maalej, *Phys. Chem. Chem. Phys.*, 2014, **16**, 22665–22676.
30 P. Xiao, Y. Guo, M. Tian, Q. Zheng, N. Jiang, X. Wu, Z. Xia and D. Lin, *Dalton Trans.*, 2015, **44**, 17366–17380.
31 H. Suo, C. Guo and T. Li, *J. Phys. Chem. C*, 2016, **120**, 2914–2924.
32 M. Liu, M. Gu, Y. Tian, P. Huang, L. Wang, Q. Shi and C. Cui, *J. Phys. Chem. C*, 2017, **5**, 4025–4033.
33 M. Back, E. Trave, P. Riello and J. J. Joos, *J. Phys. Chem. C*, 2018, **122**, 7389–7398.
34 Z. Yu, Z. Xia, E. Liu and Q. Liu, *Dalton Trans.*, 2016, **45**, 16240–16245.

